Eidgenössische Technische Hochschule Zürich

Ecole polytechnique fédérale de Zurich
Politecnico federale di Zurigo
Swiss Federal Institute of Technology Zurich

Semi-Lagrangian methods for advection of differential forms

H. Heumann, R. Hiptmair, K. Li* and J. Xu†

Research Report No. 2011-21
April 2011

Seminar für Angewandte Mathematik
Eidgenössische Technische Hochschule
CH-8092 Zürich
Switzerland

*School of Mathematical Sciences, Peking University, Beijing, China
†Department of Mathematics, PennState University, University Park, USA

Semi-Lagrangian methods for advection of differential forms

Holger Heumann, Ralf Hiptmair, Kun Li, Jinchao Xu

Abstract We study the discretization of linear transient transport problems for differential forms on bounded domains. The focus is on semi-Lagrangian methods that employ finite element approximation on fixed meshes combined with tracking of the flow map. They enjoy unconditional stability.

We derive these methods as finite element Galerkin approach to discrete material derivatives and discuss further approximations. An a priori convergence analysis is conducted and supplemented by numerical experiments.

Keywords Convection-diffusion problem, discrete differential forms, discrete Lie derivative, semi-Lagrangian methods

Mathematics Subject Classification (2000) 65M60, 65M25

1 Introduction

This article deals with transport dominated boundary value problems set in a polyhdedral Lipschitz domain $\Omega \subset \mathbb{R}^n$ and governed by a *prescribed* continuously differentiable velocity vector field $\boldsymbol{\beta} : \overline{\Omega} \mapsto \mathbb{R}^n$. To avoid technical difficulties we *assume*

$$\boldsymbol{\beta} \cdot \boldsymbol{n} = 0 \quad \text{on } \partial\Omega \,, \tag{1}$$

that is, $\boldsymbol{\beta}$ has vanishing normal components on the boundary of Ω.

Next, recall the classical linear transient 2nd-order convection-diffusion problem for an unknown scalar function $u = u(x,t)$ on a bounded polyhdedral Lipschitz domain $\Omega \subset \mathbb{R}^n$:

$$\begin{aligned} \partial_t u - \varepsilon \mathsf{div}\mathbf{grad}\, u + \boldsymbol{\beta} \cdot \mathbf{grad} u &= f \quad \text{in } \Omega\times]0,T[\,, \\ u &= 0 \quad \text{on } \partial\Omega\times]0,T[\,, \\ u(\cdot,0) &= u_0 \,. \end{aligned} \tag{2}$$

H. Heumann · R. Hiptmair
Seminar for Applied Mathematics, Swiss Federal Institute of Technology, Zurich, Switzerland
Kun Li
School of Mathematical Sciences, Peking University, Beijing, China
Jinchao Xu
Department of Mathematics, PennState University, University Park, USA

Here, f models a source and u_0 provides initial data. The parameter $\epsilon \geq 0$ controls the strength of diffusion; for $0 < \epsilon \ll 1$ the boundary value problem qualifies as *convection-dominated*.

Solving the convection-diffusion problems numerically is usually challenging in the case of dominant convection, because we encounter a singular perturbation. In the limit $\epsilon \to 0$ of vanishing diffusion the problem type changes from parabolic to hyperbolic, and the standard methods for parabolic problems usually fail.

We can distinguish two main families of methods for tackling the limiting transport problem. These are the Eulerian methods and the Lagrangian methods. The former are based on spatial discretization on a fixed mesh to which some numerical timestepping procedure is applied. Convergence and stability are guaranteed by adding certain stabilization terms as in e.g. SUPG finite element methods [18] or discontinuous Galerkin method with upwind fluxes [17, 21, 28]. Lagrangian methods dispense with a fixed spatial mesh and approximately track the flow induced by the velocity $\boldsymbol{\beta}$. Typical representatives are methods based on characteristics [3, 10, 29] and many kinds of particle methods [7].

Both principles are blended in the semi-Lagrangian approach. On the one hand it relies on fixed spatial meshes. On the other hand, transport is taken into account through explicit use of the flow map. Many variants of semi-Lagrangian methods for (2) (often for the case $\epsilon = 0$) have been proposed. Articles making substantial contributions to the numerical analysis of these methods are [9, 22, 23, 26, 27, 32].

This article as well, aims at the numerical analysis of semi-Lagrangrian methods. We go beyond the boundary value problem (2) by looking at it from the perspective of differential forms on the n-dimensional manifold Ω. Then, utilizing the notion of the *Lie derivative*, (2) turns out to be the particular instance for $p = 0$ of the following generalized convection-diffusion problems for time dependent differential p-form $\omega = \omega(t)$, $0 \leq p \leq n$

$$\begin{aligned} \varepsilon(-1)^{p+1} d * d\omega(t) + *\partial_t \omega(t) + *L_{\boldsymbol{\beta}}\omega(t) &= \varphi(t) \quad \text{in } \Omega\times]0,T[\,, \\ \iota^*\omega &= 0 \quad \text{on } \partial\Omega\times]0,T[\,, \\ \omega(0) &= \omega_0\,. \end{aligned} \tag{3}$$

Here, d is the exterior derivative and $*$ is the Hodge operator and ι^* stands for the trace of a differential form. The convection operator $L_{\boldsymbol{\beta}}$ is the Lie derivative [11, p. 133] for the prescribed velocity field $\boldsymbol{\beta}$. More explanations will be given in the next section. More details and an introduction to the calculus of differential forms in the context of discretization of partial differential equations are given in [15, Sect. 2], [2, Sect. 2], and [1, Sect. 4]. For a general introduction to differential forms see [19, Chapter V].

The correspondence between (3) and (2) is established through the concept of *Euclidean vector proxies*, which allows to model p-forms on Ω through vector fields with $\binom{n}{p}$ components, see [4, Sect. 7], [2, Table 2.1], and [16, Table 2.1][1]. For vector proxies in 3D the exterior derivative is incarnated by the classical differential operators **grad**, **curl**, and div.

A first benefit of studying the boundary value problem (3) is that, apart from (2) for $p = 0$ it also comprises the so-called magnetic convection-diffusion problem from

[1] Occasionally we will use the operator v. p. to indicate that a form is mapped to its corresponding Euclidean vector proxy

quasistatic electromagnetism in the presence of moving media for $p = 1$, see [14, Sect. 4]. In vector proxy notation the corresponding PDE reads

$$\varepsilon \mathbf{curlcurl} \boldsymbol{A} + \partial_t \boldsymbol{A} + \mathbf{curl} \boldsymbol{A} \times \boldsymbol{\beta} + \mathbf{grad}(\boldsymbol{\beta} \cdot \boldsymbol{A}) = \boldsymbol{f}. \tag{4}$$

Another benefit of the perspective of differential forms is the possibility of a unified treatment of the various cases $p = 0, \ldots, n$. This is complemented by the big advantage of the calculus of differential forms to reveal intrinsic structure, which might be blurred by the "metric overhead" carried by vector calculus.

The Galerkin discretization of (3) based on so-called discrete differential forms is presented and discussed in [14]. Here we focus on the direct semi-Lagrangian approach introduced in Sect. 3 of this article. Our main interest is in *robustness* of the methods, that is, their sustained performance in the case $\varepsilon \to 0$. The guideline is that robustness can only be expected, if the method remains viable for the limit case $\varepsilon = 0$. Therefore, we will examine only the pure advection problem

$$\begin{aligned} *\partial_t \omega(t) + *L_{\boldsymbol{\beta}} \omega(t) = \varphi(t) \quad \text{in } \Omega \times]0, T[\, , \\ \omega(0) = \omega_0 \, . \end{aligned} \tag{5}$$

Note that no inflow takes place and, thus, no boundary conditions on $\partial\Omega$ are needed.

In Sects. 2 and 3 below we recall the derivation of the semi-Lagrangian discretization of (5). For some algorithmic details we still refer to [14, Sect. 3]. The core part of the paper will then be devoted to convergence analysis and numerical studies. For fully discrete schemes and fixed polynomial degree of discrete forms we prove a priori error estimates in terms of mesh width h and timestep size τ.

Of course, for the scalar problems, e.g. $p = 0$, the methods will resemble the known semi-Lagrange Galerkin schemes [9,26] and semi-Lagrangian schemes based on interpolation [31]. We point out that for $p = 0$ we recover known convergence results [9,23,26].

Unfortunately, for the simplest lowest order discrete p-forms, $p > 0$, our theory does not predict convergence in the $L^2(\Omega)$-norm, when spatial and temporal resolution are increased in tandem, though there is ample numerical evidence for it. Numerical experiments also hint that the estimates, including those in the case $p = 0$, are not sharp. Hence, our theoretical results must be regarded as preliminary, but we hope that a more powerful theory can eventually be built on the ideas described in this article.

2 Lie derivatives and material derivatives of forms

We introduce a space-time domain $Q_T := \Omega \times [0, T]$ where $\Omega \subset \mathbb{R}^n$ and $[0, T] \subset \mathbb{R}$. We write $(x, t) \mapsto X_t(x)$, $t \in \mathbb{R}$, $x \in \Omega$, for the flow map associated with the stationary continuous vector field $\boldsymbol{\beta} : \overline{\Omega} \mapsto \mathbb{R}^n$, that is

$$\frac{d}{dt} X_t(x) = \boldsymbol{\beta}(X_t(x)) \quad \forall x \in \Omega, \ t \in \mathbb{R} \, , \quad X_0(x) = x \, . \tag{6}$$

The flow map is time-reversible, that is

$$X_t \circ X_{-t} = id \quad \forall t \in \mathbb{R} \, . \tag{7}$$

Before introducing the Lie derivative we recall the definition of the directional derivative for scalar functions $f : \Omega \mapsto \mathbb{R}$:

$$(\boldsymbol{\beta} \cdot \mathbf{grad} f)(x) := \lim_{t \to 0} \frac{f(X_t(x)) - f(x)}{t}. \tag{8}$$

Now we write $\mathcal{F}^p(\Omega)$ for the space of p-forms on Ω. The scalar functions are 0–forms and the Lie derivative $L_{\boldsymbol{\beta}}$ of higher p-form $\omega \in \mathcal{F}^p(\Omega)$ is the generalization of the directional derivative for a scalar function. For differential forms $\omega \in \mathcal{F}^p(\Omega)$ of order p, $p > 0$, we replace the point evaluation of 0-forms with integration over p-dimensional oriented sub-manifolds M_p of Ω. Then the Lie derivative of a p-form ω is [11, Ch. 4]:

$$\int_{M_p} L_{\boldsymbol{\beta}}\omega := \lim_{t\to 0} \frac{1}{t}\left(\int_{X_t(M_p)} \omega - \int_{M_p} \omega\right). \tag{9}$$

In terms of the pullback X_t^* with

$$\int_{M_p} X_t^*\omega := \int_{X_t(M_p)} \omega \tag{10}$$

we can also write

$$L_{\boldsymbol{\beta}}\omega := \lim_{t\to 0} \frac{X_t^*\omega - \omega}{t}. \tag{11}$$

With this, the Cartan's magic formula [20, p. 142, prop. 5.3] gives the following identity:

$$L_{\boldsymbol{\beta}}\omega = i_{\boldsymbol{\beta}} d\omega + d i_{\boldsymbol{\beta}}\omega, \tag{12}$$

where $i_{\boldsymbol{\beta}}$ is the contraction [11, p. 89]. For 0-forms the second term vanishes, for n-forms the first one. We refer to [5, p. 26] and [14, Rem. 1.1, 1.2] for vector proxy representations of Lie derivatives in two and three dimensional Euclidean space.

Taking into account the time dependence of the differential form $\omega = \omega(t)$, the limit value of (11) yields the so called *material derivative*:

$$D_{\boldsymbol{\beta}}\omega(t) := \lim_{\tau\to 0} \frac{X_\tau^*\omega(t+\tau) - \omega(t)}{\tau} \quad . \tag{13}$$

This derivative is the rate of change of the action of differential forms in moving media [12, p. 62]. We deduce:

$$\begin{aligned} D_{\boldsymbol{\beta}}\omega(t) &= \lim_{\tau\to 0} \frac{X_\tau^*\omega(t+\tau) - X_\tau^*\omega(t)}{\tau} + \lim_{\tau\to 0} \frac{X_\tau^*\omega(t) - \omega(t)}{\tau} \\ &= \frac{\partial}{\partial t}\omega(t) + L_{\boldsymbol{\beta}}\omega(t). \end{aligned} \tag{14}$$

In conclusion we see that our limit problem (5) is a transport problem:

$$D_{\boldsymbol{\beta}}\omega(t) = \widetilde{\varphi}(t) \quad \text{in } Q_T \quad , \quad \omega(0) = \omega_0 \ , \tag{15}$$

with $\widetilde{\varphi} := (-1)^{n(n-p)} * \varphi$, since $**\omega = (-1)^{n(n-p)}\omega$ [11, p. 364]. The explicit solution of this transport problem (15) follows from semi-group theory:

$$\int_{M_p} \omega(t) = \int_{M_p} X_{-t}^*\omega(0) + \int_0^t \left(\int_{M_p} X_{\tau-t}^*\widetilde{\varphi}(\tau)\right) d\tau \quad \forall M_p. \tag{16}$$

For $\varphi = 0$ this means, that the advected p-form ω evaluated at time t on some p-dimensional manifold M_p is equal to the value of ω at time 0 on the manifold $X_{-t}(M_p)$, i.e. the image of M_p under X_{-t}. In the case $\varphi = 0$ we find the following key conservation properties of the solution of (15):

First, closed forms remain closed when they are advected by the material derivative; if $D_{\boldsymbol{\beta}}\omega(t) = 0$ and $d\omega(0) = 0$ then $d\omega(t) = 0$, $\forall t$. This is a simple consequence of the fact that the material derivative and the exterior derivative commute $D_{\boldsymbol{\beta}} d = d D_{\boldsymbol{\beta}}$.

Second, the so-called helicity is a conserved quantity of the solution of (5). If n is odd and $p = \frac{n-1}{2}$, then

$$h_1(\omega(0)) = h_1(\omega(t)) := \int_\Omega d\omega(t) \wedge \omega(t) \tag{17}$$

for solutions of (15). If n is even and $p = \frac{n}{2}$, then we find conservation

$$h_2(\omega(0)) = h_2(\omega(t)) := \int_\Omega \omega(t) \wedge \omega(t), \quad \forall t \tag{18}$$

and

$$h_3(\omega(0)) = h_3(\omega(t)) := \int_\Omega d\omega(t) \wedge i_{\boldsymbol{\beta}}\omega(t), \quad \forall t. \tag{19}$$

For Euclidean vector proxies in $\mathbb{R}^3$ the helicity functional has the familiar form

$$h_1(\boldsymbol{A}(t)) = \int_\Omega \mathbf{curl}\boldsymbol{A}(t) \cdot \boldsymbol{A}(t)\, d\boldsymbol{x}\ .$$

The proof of (17), (18) and (19) follows from the Leibniz rule for Lie derivatives of products of p-forms ω and $n-p$ forms η [11, p. 133]:

$$d i_{\boldsymbol{\beta}}(\omega \wedge \eta) = L_{\boldsymbol{\beta}}(\omega \wedge \eta) = L_{\boldsymbol{\beta}}\omega \wedge \eta + \omega \wedge L_{\boldsymbol{\beta}} \tag{20}$$

and the assumption that the velocity field $\boldsymbol{\beta}$ has vanishing normal components on the boundary of Ω.

It goes without saying that it is very desirable to design numerical algorithms that inherit these properties and preserve closedness and helicity exactly or at least in some approximative sense.

3 Discrete differential forms

Let $\Omega_h = \{T\}$ be some simplicial triangulation of Ω. For $T \in \Omega_h$, h_T denotes the diameter and $h = \max_{T\in\Omega_h}(h_T)$. Our approach to the discretization of (15) seeks to approximate $\omega(t)$ for certain times t_k in a (fixed) space of *discrete differential forms* that are piecewise polynomial on Ω_h. Here we do not go into details, but refer to [15], [2], [1, Sect. 4] for an in-depth derivation and discussion of such spaces.

One finds finite element spaces for differential forms of any local polynomial degree. More precisely, there are basically two families $\mathcal{W}_r^p(\Omega_h)$, $r \in \mathbb{N}_0$, and $\check{\mathcal{W}}_r^p(\Omega_h)$, $r \in \mathbb{N}$, of finite element spaces, where r is related to the local polynomial degree and tells us which complete polynomial space is still contained in $\mathcal{W}_r^p(\Omega_h)$ on each simplex. Forms in these spaces have a well-defined exterior derivative and

$$\omega_h \in \mathcal{W}_r^p(\Omega_h) \quad \Rightarrow \quad d\omega_h \in \mathcal{W}_r^{p+1}(\Omega_h), \tag{21}$$

but

$$\omega_h \in \check{\mathcal{W}}_r^p(\Omega_h) \quad \Rightarrow \quad d\omega_h \in \check{\mathcal{W}}_{r-1}^{p+1}(\Omega_h). \tag{22}$$

On families of shape regular meshes, one can show standard approximation estimates [2, Theorem 5.3]:

$$\inf_{\omega_h \in \mathcal{W}_r^p} \|\omega - \omega_h\|_{0,q} \leq C h^{\min(s,r+1)} |\omega|_{s,q} \quad , \text{ if } |\omega|_{s,q} < \infty. \tag{23}$$

measured in the L^q-norm, $1 \leq q \leq \infty$, with $C > 0$ independent of h. See [15, p. 282] for the definition of Sobolev spaces and Sobolev (semi)-norms $|\cdot|_{s,q}$ of differential forms.

Further, for both families there exist so-called canonical nodal interpolation operators I_h^p [2, p. 62] commuting with the exterior derivative

$$dI_h^p \omega = I_h^{p+1} d\omega, \quad \text{for all smooth } p\text{-forms } \omega \text{ on } \Omega\ . \tag{24}$$

The interpolation operators I_h^p are built on canonical moment-based degrees of freedom of the finite element spaces $\mathcal{W}_r^p(\Omega_h)$ and $\check{\mathcal{W}}_r^p(\Omega_h)$, see [16, Sect. 3.4]. In the lowest order case of $\mathcal{W}_0^p(\Omega_h)$ these are simply the integrals $\int_{M_p} \omega$ on all p-dimensional facets M_p of all elements $T \in \Omega_h$.

In $\mathbb{R}^3$ and $\mathbb{R}^2$ the spaces $\mathcal{W}_r^p(\Omega_h)$ and $\check{\mathcal{W}}_r^p(\Omega_h)$ agree with known classical finite element spaces [2, p. 60] when we consider Euclidean vector proxies. For example, in $\mathbb{R}^3$ the spaces $\mathcal{W}_r^1(\Omega_h)$ and $\check{\mathcal{W}}_r^1(\Omega)$ are Nédélec's 1st and 2nd family of edge elements presented in [24] and [25].

In light of the conserved quantities, namely exterior derivative and helicity, it is reasonable to look for discretizations in such spaces of discrete differential forms. Discrete differential forms inherit various mathematical structures from their smooth counterparts. They are promising candidates for achieving structure preserving discretizations.

In the subsequent derivations $\mathcal{W}^p(\Omega_h)$ is a generic discrete approximation space for the space $\mathcal{F}^p(\Omega)$ of p-forms on Ω.

4 Semi-Lagrangian discretization

The pullback $X_{-\tau}^* \omega_h$ of a discrete differential form $\omega_h \in \mathcal{W}^p(\Omega_h)$ will usually fail to belong to $\mathcal{W}^p(\Omega_h)$. Thus, in order to convert the solution formula (16) into a timestepping scheme for discrete differential forms, we need to introduce an intermediate projection $P_h^p : \mathcal{F}^p(\Omega) \mapsto \mathcal{W}^p(\Omega_h)$ mapping the pullback of discrete differential forms back to the discrete space. Given such an abstract projection operator, the discrete semi-Lagrangian timestepping scheme with uniform timestep generates approximations ω_h^i to $\omega(i\tau)$ by the recursion

$$\begin{aligned} \omega_h^0 &= P_h^p \omega_0; \\ \omega_h^{i+1} &= P_h^p X_{-\tau}^* \omega_h^i + P_h^p \int_{t_i}^{t_{i+1}} X_{s-t_{i+1}}^* \widetilde{\varphi}(s) ds\ , \quad i = 0, \ldots, N-1\ . \end{aligned} \tag{25}$$

Here, we first give an abstract error analysis for this semi-Lagrangian scheme (25), under the assumption that the effect of the pullback can be controlled according to

$$\|X_{-\tau}^* \omega\|_{0,q} \leq (1 + C_e \tau) \|\omega\|_{0,q}, \tag{26}$$

with constant C_e independent of τ. We also assume a contraction property of the projection

$$\|P_h^p \omega\|_{0,q} \leq \|\omega\|_{0,q}\ . \tag{27}$$

Theorem 1 *Let $\mathcal{W}^p(\Omega_h)$ be a piecewise polynomial space of discrete differential p-forms with local polynomial degree $r \in \mathbb{N}$. $\omega \in \mathcal{F}^p(\Omega)$ and $\omega_h \in \mathcal{W}^p(\Omega_h)$ are the solutions to* (5) *and* (25)*. Further assume that*

$$\|P_h^p\omega - \omega\|_{0,q} \leq C_p h^{\min(s,r+1)}\|\omega\|_{s,q} \quad \forall \omega \in \mathcal{F}^p(\Omega),\ \|\omega\|_{s,q} < \infty \tag{28}$$

for some $1 \leq q \leq \infty$ and $s > 0$. If there holds (26) *and* (27) *then,*

$$\max_{0\leq i\leq N} \|\omega^i - \omega_h^i\|_{0,q} \leq C h^{\min(s,r+1)}(\frac{1}{\tau}+1) \max_{0\leq i\leq N} \|\omega^i\|_{s,q}, \tag{29}$$

where $\omega^i = \omega(i\tau)$ and $C > 0$ is independent of h and τ.

Proof To bound the error $\|\omega^i - \omega_h^i\|_{0,q}$ we add and substract the projection $P_h^p\omega^i$, use Cauchy-Schwarz and formulas (5) and (25):

$$\begin{aligned}
\|\omega^i - \omega_h^i\|_{0,q} &\leq \|\omega^i - P_h^p\omega^i\|_{0,q} + \|P_h^p\omega^i - \omega_h^i\|_{0,q} \\
&\leq \|\omega^i - P_h^p\omega^i\|_{0,q} + \|P_h^p X_{-\tau}^*\omega^{i-1} - P_h^p X_{-\tau}^*\omega_h^{i-1}\|_{0,q} \\
&\leq \|\omega^i - P_h^p\omega^i\|_{0,q} + (1 + C_e\tau)\|\omega^{i-1} - \omega_h^{i-1}\|_{0,q}.
\end{aligned}$$

The last inequality follows from assumptions (26) and (27). A discrete Gronwall-like inequality and the approximation assumption (28) yield with $m := \min(s, r+1)$

$$\begin{aligned}
\|\omega^i - \omega_h^i\|_{0,q} &\leq \frac{e^{C_e\tau(i-1)} - 1}{C_e\tau} \max_{1\leq j\leq i} \|\omega^j - P_h^p\omega^j\|_{0,q} + e^{C_e\tau(i-1)}\|\omega^0 - \omega_h^0\|_{0,q} \\
&\leq C_p \frac{e^{C_e\tau(i-1)} - 1}{C_e\tau} h^m \max_{1\leq j\leq i} \|\omega^j\|_{s,q} + C_p e^{C_e\tau(i-1)} h^m \|\omega^0\|_{s,q}\ ,
\end{aligned}$$

and the assertion follows.

Note that no conditions on the timestep size τ are imposed in Theorem. 1, which bears out the *unconditional stability* of semi-Lagrangian schemes, provided that the underlying projection is a contraction, *cf.* [22].

Now we examine two concrete choices of the abstract projection operator P_h^p.

1.) Interpolation scheme. A natural projection operator is the standard nodal interpolation operator for discrete differential forms [2, p. 61]. With this, the *interpolation* based semi-Lagrangian scheme reads:

$$\begin{aligned}
\omega_h^0 &= I_h^p\omega_0; \\
\omega_h^{i+1} &= I_h^p X_{-\tau}^*\omega_h^i + \int_{t_i}^{t_{i+1}} I_h^p X_{s-t_{i+1}}^*\widetilde{\varphi}(s)ds.
\end{aligned} \tag{30}$$

Unfortunately, Theorem (1) does not give convergence for most of these schemes, since the interpolation operator lacks continuity in L^q. Only for the lowest order approximation of 0-forms (functions), e.g. $r = 1$ and $p = \infty$, we have the contraction property

$$\left\|I_h^0 u\right\|_{0,\infty} \leq \|u\|_{0,\infty} \quad \forall u \in L^\infty(\Omega) \cap C^0(\Omega)\ .$$

The assumption (28) follows immediately and the standard approximation estimate (23) finally gives convergence. Nonetheless in our 2D experiments the interpolation scheme invariably converged in $L^2(\Omega)$ for $p = 1$, see Sect. 6.

2.) Galerkin projection scheme. Let $(\cdot,\cdot)_\Omega$ denote the inner product on $\mathcal{F}^p(\Omega)$

$$(\omega,\eta)_\Omega := \int_\Omega \omega \wedge *\eta, \quad \omega,\eta \in \mathcal{F}^p(\Omega)\ .$$

The L^2-orthogonal projection operator Π_h^p defined by

$$(\Pi_h^p\omega,\eta_h)_\Omega := (\omega,\eta_h) \quad \omega \in \mathcal{F}^p(\Omega), \eta_h \in \mathcal{W}^p(\Omega_h), \tag{31}$$

is another natural candidate for the abstract projection operator in (25). The resulting *Galerkin projection* semi-Lagrangian scheme is:

$$\begin{aligned}
(\omega_h^0,\eta_h)_\Omega &= (\omega_0,\eta_h)_\Omega \quad \forall \eta_h \in \mathcal{W}^p(\Omega_h);\\
(\omega_h^{i+1},\eta_h)_\Omega &= (X_{-\tau}^*\omega_h^i,\eta_h)_\Omega + \int_{t_i}^{t_{i+1}} (X_{s-t_{i+1}}^*\widetilde{\varphi}(s),\eta_h)_\Omega ds \quad \forall \eta_h \in \mathcal{W}^p(\Omega_h).
\end{aligned} \tag{32}$$

First, as is readily seen, the L^2-projection Π_h^p commutes with integration in time. Second, we clearly have a contraction property $\|\Pi_h^p\|_{0,2} \le 1$ for the projection operator, and the best approximation estimates (23) for $q = 2$ immediately yield analoguous estimates for Π_h^p. Hence, Theorem (1) gives convergence once the bounded expansion property of $\|X_{-\tau}^*\omega\|_{0,2}$ is verified. The assumption that $\boldsymbol{\beta}$ has vanishing normal components implies $X_\tau(\Omega) = \Omega$ and thus

$$\|X_{-\tau}^*\omega\|_{0,2} = \int_\Omega X_{-\tau}^*\omega \wedge *X_{-\tau}^*\omega = \int_\Omega \omega \wedge X_\tau^* * X_{-\tau}^*\omega. \tag{33}$$

In the cases $n = 2$ and $n = 3$ we can immediately deduce explicit representations of $X_\tau^* * X_{-\tau}^*$ from the known representation formulas for pullbacks (see [15, p. 245]), e.g. for differential forms ω in $\mathbb{R}^3$ with vector proxies u or $\boldsymbol{u}$ we get:

$$\begin{aligned}
p = 0: &\quad \text{v. p.}(X_\tau^* * X_{-\tau}^*\omega)(x) = \det(DX_\tau(x))u(x),\\
p = 1: &\quad \text{v. p.}(X_\tau^* * X_{-\tau}^*\omega)(x) = \det(DX_\tau(x))DX_\tau^{-1}(x)DX_\tau^{-T}(x)\boldsymbol{u}(x),\\
p = 2: &\quad \text{v. p.}(X_\tau^* * X_{-\tau}^*\omega)(x) = \det(DX_\tau(x))^{-1}DX_\tau^{T}(x)DX_\tau(x)\boldsymbol{u}(x),\\
p = 3: &\quad \text{v. p.}(X_\tau^* * X_{-\tau}^*\omega)(x) = \det(DX_\tau(x))^{-1}u(x).
\end{aligned} \tag{34}$$

In summary, we can bound $X_{-\tau}^*\omega$ by

$$\|X_{-\tau}^*\omega\|_{0,q}^2 \le C(\tau)\|\omega\|_{0,q}^2, \tag{35}$$

where the constant $C(\tau)$ depends on the Jacobian DX_τ and determinant $\det(DX_\tau)$. For smooth velocity $\boldsymbol{\beta}$ these are smooth functions of τ [13, p. 100], thus, Taylor expansion and $DX_0 = \mathrm{Id}$ yield the desired bound:

$$\|X_{-\tau}^*\omega\|_{0,q}^2 \le (1 + C_e\tau)\|\omega\|_{0,q}^2. \tag{36}$$

For the general case of p-forms in $\mathbb{R}^n$ similar bounds can be established according to the following Lemma.

Lemma 1 *For sufficiently small τ there exists C_e such that*

$$\|X_{-\tau}^*\omega\|_{0,2}^2 \le (1 + C_e\tau)\|\omega\|_{0,2}^2.$$

Proof Let vol denote the volume form on Ω, i.e. $\int_\Omega vol = |\Omega|$. A differential p-form $\omega \in \mathcal{F}^p$ at $x \in \Omega$ is a alternating p-linear map on the tangent space, i.e. here with $\Omega \subset \mathbb{R}^n$: $\omega_x : \mathbb{R}^n \times \cdots \times \mathbb{R}^n \mapsto \mathbb{R}$. Then we have [2, p. 17]

$$\|\omega\|_{0,2}^2 = \int_\Omega \omega \wedge *\omega = \int_\Omega \langle \omega_x, \omega_x \rangle vol,$$

where $\langle \cdot, \cdot \rangle$ is the innerproduct on alternating p-linear maps [2, p. 11]: For $\eta, \omega \in \mathcal{F}^p$

$$\langle \omega_x, \eta_x \rangle = \sum_\sigma \omega_x \left(\boldsymbol{e}_{\sigma(1)}, \ldots \boldsymbol{e}_{\sigma(p)} \right) \eta_x \left(\boldsymbol{e}_{\sigma(1)}, \ldots \boldsymbol{e}_{\sigma(p)} \right),$$

where the sum is over increasing sequences $\sigma : \{1, \ldots, p\} \mapsto \{1, \ldots, n\}$ and $\boldsymbol{e}_1, \ldots \boldsymbol{e}_n$ is any orthonormal basis of $\mathbb{R}^n$.

With these definitions and notations we have

$$\|X_{-\tau}^* \omega\|_{0,2}^2 = \int_\Omega X_{-\tau}^* \omega \wedge * X_{-\tau}^* \omega = \int_\Omega \langle \left(X_{-\tau}^* \omega\right)_x, \left(X_{-\tau}^* \omega\right)_x \rangle vol.$$

From the definition of the pullback it follows [2, p. 16]

$$\left(X_{-\tau}^* \omega\right)_x (\boldsymbol{e}_1, \ldots, \boldsymbol{e}_p) = \omega_{X_{-\tau}(x)} \left(DX_{-\tau}(x) \boldsymbol{e}_1, \ldots, DX_{-\tau}(x) \boldsymbol{e}_p \right)$$

and we find

$$\langle \left(X_{-\tau}^* \omega\right)_x, \left(X_{-\tau}^* \omega\right)_x \rangle = \sum_\sigma \left(\omega_{X_{-\tau}(x)} \left(DX_{-\tau}(x) \boldsymbol{e}_{\sigma(1)}, \ldots, DX_{-\tau}(x) \boldsymbol{e}_{\sigma(p)} \right) \right)^2.$$

Then p-linarity yields [30, p. 610]

$$\langle \left(X_{-\tau}^* \omega\right)_x, \left(X_{-\tau}^* \omega\right)_x \rangle = \sum_\sigma \left(\sum_{\sigma'} M^p_{\sigma',\sigma} \omega_{X_{-\tau}(x)} \left(\boldsymbol{e}_{\sigma'(1)}, \ldots, \boldsymbol{e}_{\sigma'(p)} \right) \right)^2,$$

where σ' runs over increasing sequences $\{1, \ldots, p\} \mapsto \{1, \ldots, n\}$ and $M^p_{\sigma',\sigma}$ are the p-minors of the matrix $DX_{-\tau}(x)$, i.e. the determinates of those matrices that consists of the rows $\sigma(1), \ldots, \sigma(p)$ and columns $\sigma'(1), \ldots, \sigma'(p)$ of $DX_{-\tau}(x)$. Let $\boldsymbol{M}_p$ denote that matrix that has all p-minors of $DX_{-\tau}$ as entries, then we get the bound

$$\langle \left(X_{-\tau}^* \omega\right)_x, \left(X_{-\tau}^* \omega\right)_x \rangle \leq \rho(x, \tau, p) \langle \omega_{X_{-\tau}(x)}, \omega_{X_{-\tau}(x)} \rangle,$$

where $\rho(x, \tau, p) = \rho(\boldsymbol{M}_p^T \boldsymbol{M}_p)$ is the spectral radius of $\boldsymbol{M}_p^T \boldsymbol{M}_p$. Since $DX_0(x)$ is the identity matrix we find in particular $\rho(x, 0, p) = 1$. Recall that $X_\tau(\Omega) = \Omega$ implies

$$\begin{aligned} \int_\Omega \langle \omega_{X_{-\tau}(x)}, \omega_{X_{-\tau}(x)} \rangle vol &= \int_{X_{-\tau}(\Omega)} \langle \omega_{X_{-\tau}(x)}, \omega_{X_{-\tau}(x)} \rangle vol \\ &= \int_\Omega \langle \omega_x, \omega_x \rangle X_\tau^* vol. \end{aligned}$$

Since $\mathrm{v.\,p.}(X_\tau^* vol)(x) = \det(DX_\tau(x))\, \mathrm{v.\,p.}(vol)(x)$ we get

$$\|X_{-\tau}^* \omega\|_{0,2}^2 \leq \sup_{x \in \Omega} \left(\, |\det(DX_\tau(x))| \, \rho(x, \tau, p) \, \right) \|\omega\|_{0,2}^2,$$

which yields the assertion, since $DX_\tau(x)$ is a smooth function of τ and DX_0 is the identity matrix [13, p. 100].

Remark 1 For $\tau = T$ the semi-Lagrangian schemes seem to provide $\omega(T)$ in one step. This is true, but irrelevant, because we are studying semi-Lagrangian methods as building blocks for the discretization of the convection-diffusion problem (3), see [14]. Unduly large timesteps will make the scheme miss the diffusion completely. Therefore, τ has to be linked to the spatial meshwidth h.

Remark 2 For $\tau = O(h)$ the estimates in Theorem 1 are suboptimal. In particular convergence can not be proven for $r = 0$, although it is suggested by our experiments. This phenomenon is also observed for Lagrangian methods of scalar transport problems. Up to our knowledge there exists no proof of convergence for the case $r = 0$, except for certain simplified problems in $\mathbb{R}^1$ and $\mathbb{R}^2$ with constant velocity [23].

5 Fully discrete semi-Lagrangian schemes

An actual implementation of schemes (32) and (30) requires further approximations. This needs to be done very carefully in order to preserve the favourable stability properties of Lagrangian schemes established in Theorem 1. A family of simplicial meshes $(\Omega_h)_h$ with mesh width h is taken for granted.

(i) Approximate flow map. First we would like to introduce approximations $\bar{X}_\tau$ of the flow map X_τ that depend on both Ω_h and the timestep τ. We require consistency in the following sense:

- $\bar{X}_\tau : \Omega \mapsto \Omega$ is Ω_h-piecewise smooth,
- there are $k, l \geq 1$ such that for $h \to 0$ and $\tau \to 0$

$$\|X_\tau - \bar{X}_\tau\|_\infty \leq O(h^{k+1}\tau + \tau^l) \quad \text{and} \quad \|X_\tau - \bar{X}_\tau\|_{1,\infty} \leq O(h^k\tau + \tau^l). \tag{37}$$

A simple construction of approximate flow maps relies on the nodal basis functions $(\lambda_i)_i$ spanning the space of continuous piecewise polynomial Lagrangian finite element functions of degree k. The degrees of freedom associated to these basis functions are point evaluations at particular nodal points $(\boldsymbol{a}_i)_i$ defined by affine coordinates inside the simplices of the mesh. Then we define

$$\bar{X}_\tau(\boldsymbol{x}) := \sum_i \bar{X}_{\tau,i}\lambda_i(\boldsymbol{x}) \tag{38}$$

where the coefficients $\bar{X}_{\tau,i}$ are approximations to the trajectories $X_\tau(\boldsymbol{a}_i)$ of the degrees of freedoms $\boldsymbol{a}_i$ with

$$\|X_\tau(\boldsymbol{a}_i) - \bar{X}_{\tau,i}\| \leq O(\tau^l) \quad \text{for} \quad \tau \to 0\,, \tag{39}$$

see figure 1 for an illustration.

This approximation is consistent by construction. The error $|X_\tau - \bar{X}_\tau|_{s,\infty}$ splits into an error originating from approximations of the trajectories of the degrees of freedom, which is assumed to be of order $O(\tau^l)$, and an error originating from interpolation in Lagrangian finite element functions. The bound on the interpolation error follows from standard interpolation estimates for Lagrangian finite elements [6, Sect. 3.1]. If Π_h denotes the interpolation operator and $\boldsymbol{\beta}$ is sufficiently smooth, we have:

$$\begin{aligned}\|X_\tau - \Pi_h X_\tau\|_{s,\infty} &= \|X_\tau - \mathrm{id} - \Pi_h(X_\tau - \mathrm{id})\|_{s,\infty} \\ &\leq Ch^{k+1-s}|X_\tau - \mathrm{id}\,|_{k+1,\infty} \\ &\leq Ch^{k+1-s}\tau|\boldsymbol{\beta}|_{k+1,\infty},\end{aligned}$$

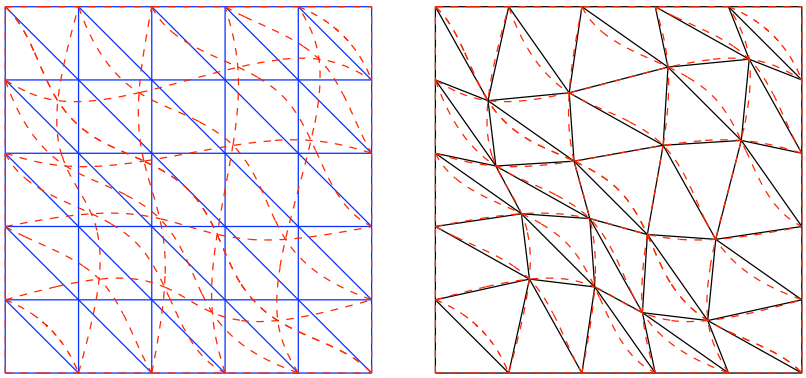

Fig. 1 Illustration of the approximation of the flow map X_τ. Left: The fixed mesh Ω_h (blue solid lines) and its image $X_\tau(\Omega_h)$ (red dashed lines) under the exact flow. For smooth $\boldsymbol{\beta}$ $X_\tau(\Omega_h)$ consists of non-polynomial curved polygons. Right: A low order consistent approximation $\bar{X}_\tau(\Omega_h)$ (black solid lines) of $X_\tau(\Omega_h)$ (red dashed lines). Here we used linear Lagrangian elements and exact trajectories for the vertices, hence $\bar{X}_\tau(\Omega_h)$ has again straight edges and the vertices of $X_\tau(\Omega_h)$ and $\bar{X}_\tau(\Omega_h)$ coincide.

where the last inequality follows from (6).

(ii) Approximation of the source. We have to approximate the time integration of the right-hand side in (32) and (30). Since φ does not depend on ω, it is reasonable to chose some quadrature method for the approximation $Q(\varphi, t, t+\tau) \approx \int_t^{t+\tau} \varphi(s)ds$ which satisfies

$$\left| \int_t^{t+\tau} \varphi(s)ds - Q(\varphi, t, \tau) \right| \leq C\tau^m \max_{t\leq s\leq t+\tau} \left| \frac{d^m}{dt^m}\varphi(s) \right|, \quad m \geq 1\,. \tag{40}$$

Now we are in a position to formulate fully discrete semi-Lagrangian timestepping schemes.

1.) Fully discrete Galerkin projection scheme. Find $\omega_h^i \in \mathcal{W}^p(\Omega_h)$, $i = 0, \ldots, N$, such that for all $\eta_h \in \mathcal{W}^p(\Omega_h)$:

$$\begin{aligned} (\omega_h^0, \eta_h)_\Omega &= (\omega_0, \eta_h)_\Omega; \\ (\omega_h^{i+1}, \eta_h)_\Omega &= (\bar{X}^*_{-\tau}\omega_h^i, \eta_h)_\Omega + (Q(\bar{X}^*_{s-t_{i+1}}\widetilde{\varphi}(s), t_i, t_{i+1}), \eta_h)_\Omega. \end{aligned} \tag{41}$$

For $p = 0$ and continuous piecewise linear approximation spaces (41) is exactly the scheme in [27].

2.) Fully discrete interpolation scheme. Find $\omega_h^i \in \mathcal{W}^p(\Omega_h)$, $i = 0, \ldots, N$, such that:

$$\begin{aligned} \omega_h^0 &= I_h^p \omega_0; \\ \omega_h^{i+1} &= I_h^p \bar{X}^*_{-\tau}\omega_h^i + I_h^p Q(\bar{X}^*_{s-t_{i+1}}\widetilde{\varphi}(s), t_i, t_{i+1}) \end{aligned} \tag{42}$$

Owing to the approximation (38) of the flow map, the pullbacks are still piecewise polynomial. Hence, the right-hand sides in (41) and (42) can be computed exactly. For instance, for the Galerkin projection scheme (41) this can be done after the intersections of all elements T of the mesh Ω_h with all elements $\bar{X}_\tau(T')$ of the transported mesh $\bar{X}_\tau(\Omega_h)$ have been found (see Figure 2 for illustration).

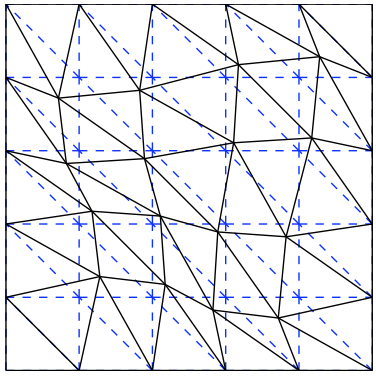

Fig. 2 The innerproducts on the right-hand side of the Galerkin projection scheme (41) pair finite element functions defined on two different meshes, namely the fixed mesh (blue dashed lines) and the approximated transported mesh (black solid lines). Since in both meshes the facets are polynomial, we can algorithmically determine a partitioning of Ω such that all appearing finite element functions are smooth on each part. The finite element functions and the pullbacks are polynomials, hence the innerproducts can be computed exactly.

At a first glance this seems to be very expensive. Nevertheless we contend that at least for the case of low order approximations ($k = 0$) such schemes provide competitive methods.

The interpolation schemes (42) are cheaper in certain cases. In particular, in the case of lowest order approximation and $p < n$ the degrees of freedom are simple facet integrals and we only need to determine intersections of transported p-dimensional facets with elements T of mesh Ω_h. In addition, the interpolation schemes give entirely explicit schemes, while for the Galerkin projection schemes we have to solve a linear system in each timestep. Algorithmic details for interpolation schemes are discussed in [14, Sect. 3].

Remark 3 Inspired from standard finite element techniques one could be tempted to split the inner product $(\bar{X}^*_{-\tau}\omega_h, \eta_h)_\Omega$ into a sum of integrals over elements of Ω_h and apply some quadrature rule there. We dub this scheme the **quadrature-based scheme**:

Find $\omega_h^i \in \mathcal{W}^p(\Omega_h)$, $i = 0, \dots, N$, such that for all $\eta_h \in \mathcal{W}^p(\Omega_h)$:

$$\begin{aligned} (\omega_h^0, \eta_h)_{\Omega,h} &= (\omega_0, \eta_h)_{\Omega,h}; \\ (\omega_h^{i+1}, \eta_h)_{\Omega,h} &= (\bar{X}^*_{-\tau}\omega_h^i, \eta_h)_{\Omega,h} + (Q(\bar{X}_{s-t_{i+1}}\widetilde{\varphi}(s), t_i, t_{i+1}), \eta_h)_{\Omega,h} \,, \end{aligned} \tag{43}$$

with

$$(\omega, \eta)_{\Omega,h} = \sum_{T\in\Omega_h} \sum_i w_{i,T} * \omega(x_{i,T}) \wedge \eta(x_{i,T}) \tag{44}$$

for suitable quadrature points $(x_{i,T})_i \in T$ and quadrature weights $(w_{i,T})_i$. Compared to the projection scheme this reduces the computational cost, since only the trajectories for the quadrature points need to be computed. However, this scheme is dubious since we apply quadrature on domains with discontinuous integrands. Our experiments in the next section (see Example 2) show that these doubts are justified.

In analogy to Theorem 1 we can prove convergence for the solutions of the Galerkin projection scheme (41). To begin with, for sufficiently smooth velocity $\boldsymbol{\beta}$ our consistent approximations of the flow map fulfill

$$\|X^*_{-\tau}\omega - \bar{X}^*_{-\tau}\omega\|_{0,2} \leq C_f(h^k\tau + \tau^l)\|\omega\|_{1,2}\,, \tag{45}$$

for $C_f = C_f(\boldsymbol{\beta}, D\boldsymbol{\beta}) > 0$ independent of h and τ.

Lemma 2 *Assume the velocity field $\boldsymbol{\beta}$ fulfils $\|\boldsymbol{\beta}\|_{l+1,\infty} \leq \infty$. Then a consistent approximation of the flow map according to* (38) *fulfills* (45).

Proof The proof uses similar arguments as the proof of Lemma 1. With the notation introduced there, we have in particular

$$\|X^*_{-\tau}\omega - \bar{X}^*_{-\tau}\omega\|^2_{0,2} = \int_\Omega \left\langle \left(X^*_{-\tau}\omega - \bar{X}^*_{-\tau}\omega\right)_x, \left(X^*_{-\tau}\omega - \bar{X}^*_{-\tau}\omega\right)_x \right\rangle vol.$$

In what follows σ and σ' are increasing sequences $\{1,\dots,p\} \mapsto \{1,\dots,n\}$ and $\boldsymbol{e}_1,\dots,\boldsymbol{e}_n$ is an orthonormal basis of $\mathbb{R}^n$. For fixed $x \in \Omega$ and τ we introduce the abbreviations $\omega_x(\boldsymbol{e}_\sigma) := \omega_x\left(\boldsymbol{e}_{\sigma(1)},\dots,\boldsymbol{e}_{\sigma(p)}\right)$, $\omega_X := \omega_{X_{-\tau}(x)}$ and $DX := DX_{-\tau}(x)$. Then we find

$$\left(X^*_{-\tau}\omega\right)_x(\boldsymbol{e}_\sigma) = \omega_X(DX\boldsymbol{e}_\sigma) = \sum_{\sigma'} M^p_{\sigma',\sigma}\omega_X(\boldsymbol{e}_\sigma)$$

and

$$\left(\bar{X}^*_{-\tau}\omega\right)_x(\boldsymbol{e}_\sigma) = \omega_{\bar{X}}\left(D\bar{X}\boldsymbol{e}_\sigma\right) = \sum_{\sigma'} \bar{M}^p_{\sigma',\sigma}\omega_{\bar{X}}(\boldsymbol{e}_\sigma)\,,$$

where $M^p_{\sigma,\sigma'}$ and $\bar{M}^p_{\sigma,\sigma'}$ are the p-minors of DX and $D\bar{X}$. Together this yields

$$\left(X^*_{-\tau}\omega - \bar{X}^*_{-\tau}\omega\right)_x(\boldsymbol{e}_\sigma) = \omega_X(DX\boldsymbol{e}_\sigma) - \omega_{\bar{X}}\left(D\bar{X}\boldsymbol{e}_\sigma\right) = A_1 + A_2$$

with

$$A_1 = \sum_{\sigma'}\left(M^p_{\sigma',\sigma} - \bar{M}^p_{\sigma',\sigma}\right)\omega_X(\boldsymbol{e}_{\sigma'})$$

and

$$A_2 = \sum_{\sigma'}\bar{M}^p_{\sigma',\sigma}\left(\omega_X(\boldsymbol{e}_{\sigma'}) - \omega_{\bar{X}}(\boldsymbol{e}_{\sigma'})\right).$$

For each σ' we have that $\omega_X(\boldsymbol{e}_{\sigma'})$ is function of X, i.e. for smooth differential forms Taylor expansion yields

$$\omega_X(\boldsymbol{e}_{\sigma'}) = \omega_{\bar{X}}(\boldsymbol{e}_{\sigma'}) + (X - \bar{X})\partial_x\omega_x(\boldsymbol{e}_{\sigma'})_{|x=X+s(X-\bar{X})}$$

for some s with $0 \leq s \leq 1$. As in the proof of Lemma (1) the matrices containing the p-minors of DX and $D\bar{X}$ shall be denoted by $\boldsymbol{M}_p$. Thus, we have

$$\|X^*_{-\tau}\omega - \bar{X}^*_{-\tau}\omega\|^2_{0,2} \leq a_1 + a_2,$$

with

$$a_1 = \sup_x \rho\left((\boldsymbol{M}_p - \bar{\boldsymbol{M}}_p)^T(\boldsymbol{M}_p - \bar{\boldsymbol{M}}_p)\right)\sup_x|\det(DX_\tau)|\|\omega\|^2_{0,2}$$

and

$$a_2 = \sup_x \rho\left(\bar{\boldsymbol{M}}_p^T\bar{\boldsymbol{M}}_p)\right)\sup_x|\det(DX_\tau)|\|X - \bar{X}\|^2_{0,\infty}|\omega|^2_{1,2}.$$

We get the bound

$$\|X^*_{-\tau}\omega - \bar{X}^*_{-\tau}\omega\|^2_{0,2} \leq C\|X_{-\tau} - \bar{X}_{-\tau}\|^2_{1,\infty}\|\omega\|^2_{0,2} + C\|X_{-\tau} - \bar{X}_{-\tau}\|^2_{0,\infty}|\omega|^2_{1,2},$$

and the assertion follows.

Theorem 2 *Let ω_h be the solution of (41) with either $\mathcal{W}^p(\Omega_h) = \mathcal{W}^p_r(\Omega)$,$r \geq 0$, or $\mathcal{W}^p(\Omega_h) = \check{\mathcal{W}}^p_r(\Omega_h)$, $r > 0$. Assume*

- *that the solution $\omega(t) \in \mathcal{F}^p(\Omega)$ of (3) satisfies $\|\omega\|_{s,2} < \infty$ for $s \geq 1$ and all $0 \leq t \leq T$,*
- *the expansion property (26) for the exact flow map,*
- *order m approximation of the source according to (40).*

Then for h and τ sufficiently small it is

$$\begin{aligned}\max_{0\leq i\leq N} \|\omega^i - \omega_h^i\|_{0,2} \leq & C\left((1+\frac{1}{\tau})h^{\min(s,r+1)} + h^k + \tau^{l-1}\right) \max_{0\leq i\leq N} \|\omega^i\|_{s,2} \\ & + C(\tau^{m-1} + \tau h^k + \tau^l)C(\widetilde{\varphi})\end{aligned} \tag{46}$$

where $\omega^i = \omega(i\tau)$.

Proof The proof is similar to the proof of Theorem 1. The additional approximations, the approximate flow and the approximation of the source, give additional consistency errors in the error recursion for the error:

$$\begin{aligned}\|\omega^i - \omega_h^i\|_{0,2} \leq & \|\omega^i - \Pi_h^p \omega^i\|_{0,2} + \|\Pi_h^p \omega^i - \omega_h^i\|_{0,2} \\ \leq & \|\omega^i - \Pi_h^p \omega^i\|_{0,2} + \|\Pi_h^p X^*_{-\tau}\omega^{i-1} - \Pi_h^p \bar{X}^*_{-\tau}\omega_h^{i-1}\|_{0,2} \\ & + \|\Pi_h^p \int_{t_{i-1}}^{t_i} X^*_{s-t_i}\widetilde{\varphi}(s)ds - \Pi_h^p Q(\bar{X}^*_{s-t_i}\widetilde{\varphi}(s), t_{i-1}, t_i)\|_{0,2} \\ := & E_1 + E_2 + E_3.\end{aligned}$$

For the second term in the last line we find by L^2-stability, bound (26), bound (45) and $l \geq 1$:

$$\begin{aligned}E_2 \leq & \|X^*_{-\tau}\omega^{i-1} - \bar{X}^*_{-\tau}\omega_h^{i-1}\|_{0,2} \\ \leq & \|\bar{X}^*_{-\tau}\omega^{i-1} - \bar{X}^*_{-\tau}\omega_h^{i-1}\|_{0,2} + \|(X^*_{-\tau} - \bar{X}^*_{-\tau})\omega^{i-1}\|_{0,2} \\ \leq & (1 + C_e\tau)\|\omega^{i-1} - \omega_h^{i-1}\|_{0,2} + C_f(h^k\tau + \tau^l)\|\omega^{i-1}\|_{1,2}.\end{aligned}$$

For the term E_3 we get from bound (45) and the approximation of the source:

$$\begin{aligned}E_3 \leq & \|\int_{t_{i-1}}^{t_i} X^*_{s-t_i}\widetilde{\varphi}(s)ds - Q(\bar{X}^*_{s-t_i}\widetilde{\varphi}(s), t_{i-1}, t_i)\|_{0,2} \\ \leq & \|\int_{t_{i-1}}^{t_i} \bar{X}^*_{s-t_i}\widetilde{\varphi}(s)ds - Q(\bar{X}^*_{s-t_i}\widetilde{\varphi}(s), t_{i-1}, t_i)\|_{0,2} \\ & + \|\int_{t_{i-1}}^{t_i} \bar{X}^*_{s-t_i}\widetilde{\varphi}(s)ds - \int_{t_{i-1}}^{t_i} X^*_{s-t_i}\widetilde{\varphi}(s)ds\|_{0,2} \\ \leq & C_1(\widetilde{\varphi})h^m + C_2(\widetilde{\varphi})(h^k\tau^2 + \tau^{l+1}),\end{aligned}$$

with $C_1(\widetilde{\varphi})$ and $C_2(\widetilde{\varphi})$ independent of h and τ. Then discrete Gronwall-like inequality yields:

$$\begin{aligned}\|\omega^i - \omega_h^i\|_{0,2} \leq & \frac{e^{C_e\tau(i-1)} - 1}{C_e\tau} \max_{1\leq j\leq i} \left(\|\omega^j - \Pi_h^p\omega^j\|_{0,2} + C_f(h^k\tau + \tau^l)\|\omega^{j-1}\|_{1,2}\right) \\ & + \frac{e^{C_e\tau(i-1)} - 1}{C_e\tau}(\tau^m + \tau^2 h^k + \tau^{l+1})C(\varphi) \\ & + e^{C\tau(i-1)}\|\omega^0 - \omega_h^0\|_{0,2}\end{aligned}$$

and the assertion follows.

Since (26) cannot hold for the interpolation operators I_h^p, a counterpart of Theorem. 2 remains elusive for the interpolation scheme (42). However, if we had a convergence estimate for all p in some norm, this would involve an estimate for $d(\omega^i - \omega_h^i)$ in the same norm. This could be concluded from the commuting diagram property (24).

This commuting property is also very important for analyzing whether the discrete schemes inherit the preservation of closedness or helicity. While the interpolation schemes obviously preserve closedness of initial data in the case of vanishing righthand side φ, this cannot be expected from the Galerkin projection scheme.

The following lemma proves, that the interpolation schemes preserve helicity approximatively, e.g. the error converges with the same rate as the error of the solution.

Lemma 3 *Let ω be the solution of (3) with $\varphi = 0$ and assume that the solution $\omega_h(T)$ of the interpolation scheme (42) satiesfies for all $p \in \{0, \dots, n\}$ and some $s > 1$*

$$\|\omega(0) - \omega_h(0)\|_{0,q} \leq Ch^s \quad \textit{and} \quad \|\omega(T) - \omega_h(T)\|_{0,q} \leq Ch^s \ . \tag{47}$$

with $C > 0$ independent of h and ω. Then

$$|h_i(\omega_h(0)) - h_i(\omega_h(T))| \leq Ch^s \ . \tag{48}$$

where h_i, $i = 2, 3$ for even n,$i = 1$ for odd n, stands for the helicity functionals defined in (17), (18) and (19).

Proof We give the proof for helicity h_1. For h_2 and h_3 the assertion follows in the same way. Note that $h_1(\omega(0)) - h_1(\omega(T)) := h_1(\omega^0) - h_1(\omega^N) = 0$, then

$$\begin{aligned}
|h_1(\omega_h^0) - h_1(\omega_h^N)| =& |h_1(\omega_h^0) - h_1(\omega^0) + h_1(\omega^N) - h_1(\omega h^N)| \\
=& \left| \int_\Omega d\omega_h^0 \wedge \omega_h^0 - d\omega^0 \wedge \omega^0 + d\omega^N \wedge \omega^N - d\omega_h^N \wedge \omega_h^N \right| \\
\leq& \left| \int_\Omega (d\omega_h^0 - d\omega^0) \wedge \omega_h^0 \right| + \left| \int_\Omega d\omega^0 \wedge (\omega_h^0 - \omega^0) \right| \\
&+ \left| \int_\Omega (d\omega^N - d\omega_h^N) \wedge \omega^N \right| + \left| \int_\Omega d\omega^N \wedge (\omega^N - \omega_h^N) \right|
\end{aligned}$$

The assertion follows by Cauchy-Schwarz-inequality and the fact that the exterior derivatives of solutions of the interpolation schemes converge of same order as the solutions themselves.

6 Numerical examples: 1-forms in $\mathbb{R}^2$

In this section we take $\Omega = \mathbb{R}^2$ and study the performance of semi-Lagrangian methods for the transport problem

$$\begin{aligned}
*\partial_t \omega(t) + *L_{\mathcal{B}}\omega(t) = \varphi \quad \text{in } \Omega \subset \mathbb{R}^2 \ , \\
\omega(0) = \omega_0
\end{aligned} \tag{49}$$

for time-dependent 1-forms $\omega(t) \in \mathcal{F}^1(\Omega)$. In vector proxy notion with $\mathbf{u} := \mathrm{v.\,p.}(\omega)$ this reads

$$\begin{aligned} \partial_t \mathbf{u} + \mathbf{grad}(\boldsymbol{\beta} \cdot \mathbf{u}) + \boldsymbol{R}^T \mathsf{div}(\boldsymbol{R}\mathbf{u})\boldsymbol{\beta} = \mathbf{f} \quad \text{in } \Omega\,, \\ \mathbf{u}(0) = \mathbf{u}_0 \text{ in } \Omega, \end{aligned} \tag{50}$$

with $\mathbf{R} = \begin{pmatrix} 0 & 1 \\ -1 & 0 \end{pmatrix}$. We approximate ω by lowest order discrete 1-forms $\omega_h \in \mathcal{W}_0^1(\Omega_h)$ on a triangular mesh Ω_h. In the following we will study the performance of the *Galerkin projection* schemes 41 and the *interpolation* schemes 42. The discrete space $\mathcal{W}_0^1(\Omega_h)$ consists of tangentially continuous, piecewise polynomial functions, with piecewise constant exterior derivatives ("edge elements"). The basis functions are associated with the edges of the mesh and the degrees of freedom are line integrals on edges.

Further, we use continuous piecewise linear Lagrangian finite elements to approximate the flow map (38). If not stated differently, we use explicit Euler timesteps to determine the flow of the vertices. Thus, the transported mesh $\bar{X}_\tau(\Omega_h)$ is again a mesh with straight edges. The inner products for both, the Galerkin projection scheme and the interpolation scheme, are calculated exactly. The right-hand sides are evaluated by means of one-point quadrature in time, using the endpoint of the integration interval (40). In the following experiments we link the timestep size τ to the meshsize h by the relationship

$$\tau = \gamma \frac{h}{\|\boldsymbol{\beta}\|}, \tag{51}$$

where γ is some constant. In most cases, we will choose $\gamma \approx 1$, which is advisable for the full advection-diffusion problem in a setting with (locally) significant diffusion. Remember that it is this class of problems that we aim to design methods for. Nevertheless, for the sake of brevity and clarity, we do not treat diffusion terms here.

6.1 Example 1: Generic right-hand side

In (50), we consider $\Omega = [-1, 1]^2$ and choose the velocity

$$\boldsymbol{\beta} = (1 - x_1^2)(1 - x_2^2) \begin{pmatrix} 0.66 \\ 1 \end{pmatrix}.$$

The date $\mathbf{u}(0)$ and f is chosen such that

$$\boldsymbol{u} = \cos(2\pi t) \begin{pmatrix} \sin(\pi x_1) \sin(\pi x_2) \\ (1 - x_1^2)(1 - x_2^2) \end{pmatrix}.$$

is the solution. With this choice we encounter a non-zero right-hand side in (50).

In Figure 3 we monitor the convergence for different values of γ. The numerical error of the interpolation scheme and the projection scheme are almost the same. Since we observe convergence here, we conclude that our estimate in Theorem 2 is not sharp.

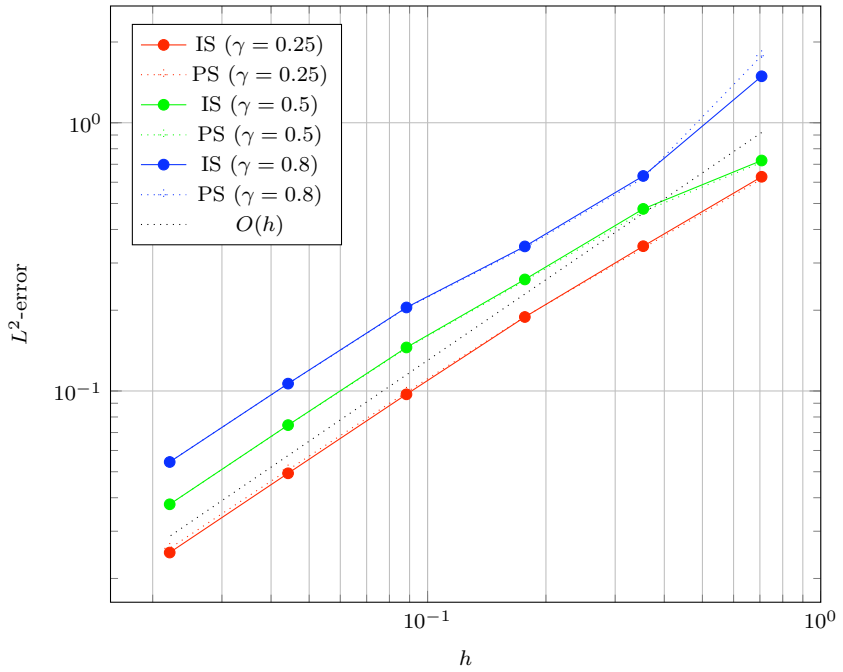

Fig. 3 Example 1: Convergence rates of L^2-error at $t = 0.4$ for the interpolation scheme (IS) and the Galerkin projection scheme (PS) on time interval $[0, 0.4]$ for $\gamma = 0.25$, $\gamma = 0.5$ and $\gamma = 0.8$.

6.2 Example 2: Failure of quadrature based scheme

The drawback of the Galerkin projection scheme obviously is the requirement to calculate the inner products $(\bar{X}^*_{-\tau}\omega_h, \eta_h)_\Omega$ exactly. A cheaper option is the quadrature-based scheme introduced in remark 3.

We consider the same data for problem (50) as in example 1. Figure 4 shows the convergence rate of a quadrature-based scheme built on the barycenters as quadrature points. Only for a few initial refinement steps there is some sort of convergence, breaking down when we refine further. We observe the same phenomenon, if we use higher order quadrature rules to approximate the inner products (see Figure 5). This result is as expected since the quadrature-based scheme applies quadrature on domains with discontinuous integrands.

6.3 Example 3: Rotating hump problem

Now we study the behaviour of the interpolation scheme (42) and the projection scheme (41) for the classical rotating hump problem [8, Sect. 5.1]. We consider problem (50) on a circular domain $\Omega := \{(x_1, x_2) : x_1^2 + x_2^2 \leq 1\}$ with source term $\boldsymbol{f} = 0$, the velocity field:

$$\boldsymbol{\beta} = \begin{pmatrix} x_2 \\ -x_1 \end{pmatrix} \tag{52}$$

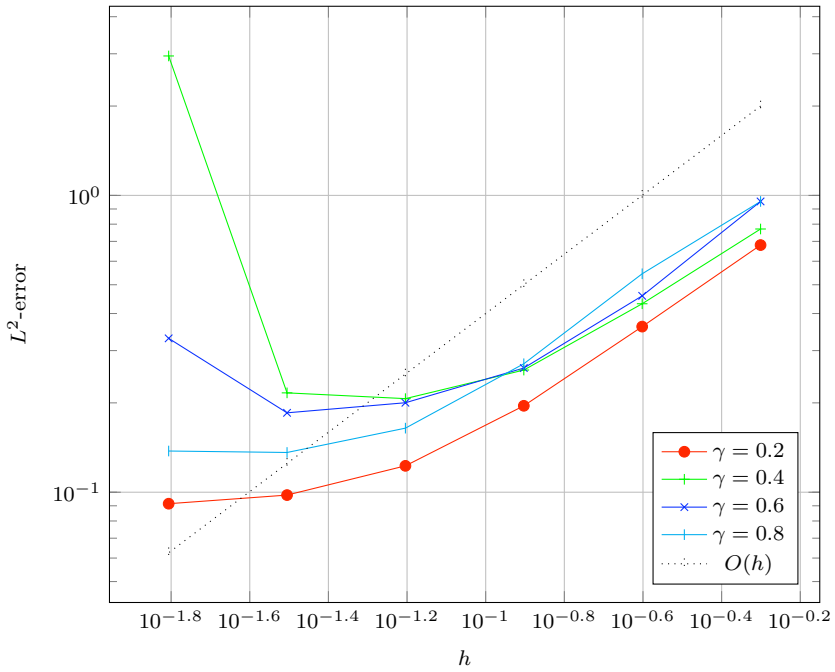

Fig. 4 Example 2: Convergence rate of the L^2-error at $t-0.4$ for a Galerkin scheme with low order quadrature on the time interval $[0, 0.4]$ and $\gamma = 0.2$, $\gamma = 0.4$, $\gamma = 0.6$ and $\gamma = 0.8$.

and "smooth hump" initial data

$$\boldsymbol{u}_0(\boldsymbol{x}) = \begin{cases} \operatorname{grad} f(\boldsymbol{x}) & \text{, for } \sqrt{x_1^2 + (x_2 - 0.25)^2} \leq 0.5 \\ (0,0)^T & \text{, for } \sqrt{x_1^2 + (x_2 - 0.25)^2} > 0.5 \end{cases} , \in C^2(\Omega) . \tag{53}$$

with the function

$$f(\boldsymbol{x}) = \cos\left(\pi \sqrt{x_1^2 + (x_2 - 0.25)^2}\right)^4 . \tag{54}$$

The exact solution is

$$\boldsymbol{u}(t, \boldsymbol{x}) = (\boldsymbol{R}(t))^{-1} \boldsymbol{u}_0(\boldsymbol{R}(t)\boldsymbol{x}), \quad \boldsymbol{R}(t) := \begin{pmatrix} \cos(t) & -\sin(t) \\ \sin(t) & \cos(t) \end{pmatrix} . \tag{55}$$

In order to study the impact of the approximation of the flow map, we use both (i) the explicit Euler method, and (ii) the explicit midpoint method in order to determine the positions of the vertices of the advected mesh, *cf.* (38). Final time is $T = 2\pi$, that is, we track one full revolution. Tables 1, 2, 3, 4 list the L^2 errors of numerical solutions at $T = 2\pi$ for different mesh sizes h and timestep sizes τ. The numbers convey the need for balancing h and τ, with higher order integration of trajectories allowing larger timesteps. First, for fixed meshsize h we observe that the minimal error is not attained for the minimal timestep size, but for some medial values of τ. This observation matches the negative power of τ in the estimate of Theorem (2).

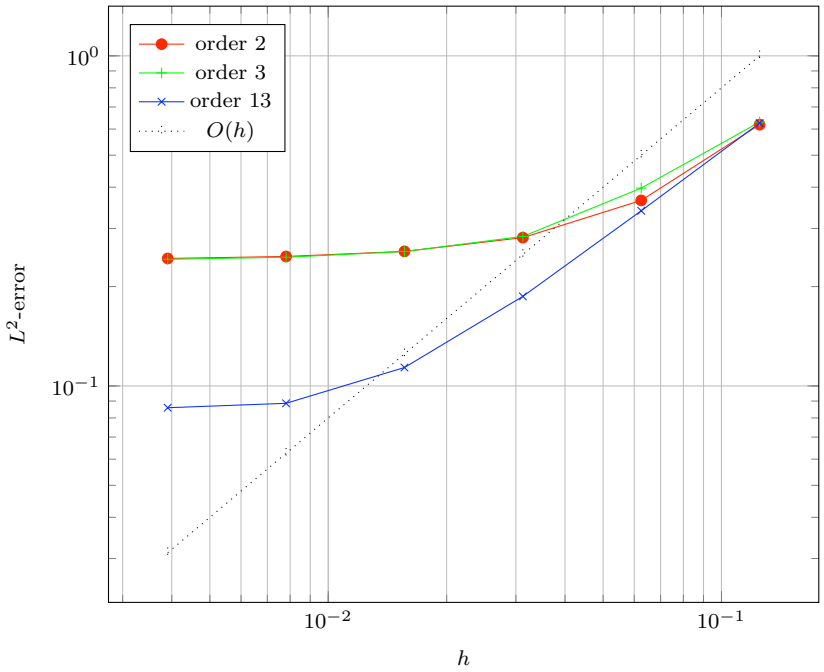

Fig. 5 Example 2: Convergence rate of the L^2-error at $t - 0.4$ for a Galerkin scheme with local quadrature rules of different orders on the time interval $[0, 0.4]$.

$\tau \backslash h$	0.420	0.210	0.105	0.052	0.026
1.5707	1.86	1.89	1.86	1.88	2.33
0.7853	1.86	1.88	1.88	2.01	2.36
0.3926	1.84	1.82	1.80	2.01	2.32
0.1963	1.85	1.79	1.52	1.51	1.79
0.0997	1.85	1.80	1.54	1.05	1.02
0.0498	1.85	1.81	1.59	1.18	0.63
0.0249	1.85	1.81	1.61	1.26	0.79
0.0124	1.85	1.81	1.62	1.30	0.88
0.0062	1.85	1.81	1.63	1.31	0.92

Table 1 Example 3, rotating hump: L^2-error of the solution of the **interpolation scheme** (42) with explicit Euler method for different discretization parameters timestep τ (rows) and mesh size h (columns).

Second, when comparing the errors for the two integration schemes, we see that the minimal error for the explicit midpoint method is attained for larger values of τ than for the explicit Euler method. This reflects the higher order approximation properties of the explicit midpoint method, that appear explicitly in the estimate of Theorem 2 for the projection scheme.

For our choice of data we find that the solution fulfills $\mathsf{div}\boldsymbol{Ru} = 0$ for all times, which we expect to hold also for the numerical solution produced by the interpolation scheme. Yet, when using the explicit midpoint rule for tracking vertex trajectories. This is only true for small timesteps and fine meshes as can be seen from Figure 7 On the other hand, the scheme based on explicit Euler seems immune to "div-pollution".

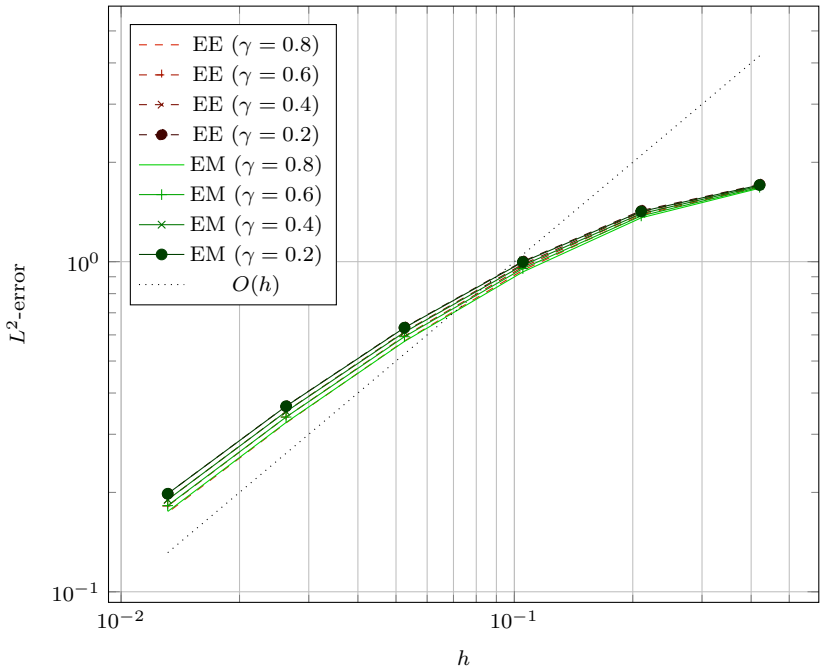

Fig. 6 Example 3: Convergence rates of L^2-error at $t = 0.5\pi$ for the interpolation scheme with explicit midpoint rule (MM) and explicit Euler method (EE) on time interval $[0, 0.5\pi]$ for $\gamma = 0.2$, $\gamma = 0.4$, $\gamma = 0.6$ and $\gamma = 0.8$.

$\tau \backslash h$	0.420	0.210	0.105	0.052	0.026
1.5707	1.85	1.86	1.91	2.12	2.47
0.7853	1.79	1.53	1.51	1.70	1.80
0.3926	1.83	1.56	0.99	0.55	0.50
0.1963	1.84	1.72	1.23	0.60	0.22
0.0997	1.84	1.77	1.49	0.85	0.33
0.0498	1.85	1.79	1.56	1.15	0.52
0.0249	1.85	1.80	1.59	1.24	0.79
0.0124	1.85	1.81	1.61	1.28	0.87
0.0062	1.85	1.81	1.62	1.31	0.92

Table 2 Example 3, rotating hump: L^2-error of the solution of the **interpolation scheme** (42) with explicit midpoint method for different discretization parameters timestep τ (rows) and mesh size h (columns).

We blame this puzzling observation on the fact that the approximate flow maps will not map Ω exactly onto itself; backward trajectories may leave the domain and there may be edges, whose image under the flow will be at least partly outside the fixed mesh. In our implementation of the interpolant $\Pi_h \bar{X}^*_{-\tau} \omega_h$ we simply ignore the contribution of such edges, thus destroying the closedness property, see Figures 8. As long as ω_h has compact support away from $\partial\Omega$ this effect remains invisible. Yet, inevitable artificial diffusion will make $\operatorname{supp} \omega_h$ spread, reach $\partial\Omega$, and interpolation errors will pollute $d\omega_h$, see Figure 7. Perversely, this happens for the midpoint rule but not in the case of

$\tau\backslash h$	0.420	0.210	0.105	0.052	0.026
1.5707	1.85	1.86	1.90	2.11	2.45
0.7853	1.85	1.85	1.87	2.02	2.32
0.3926	1.84	1.80	1.78	1.99	2.29
0.1963	1.84	1.79	1.57	1.49	1.75
0.0997	1.84	1.80	1.60	1.18	1.01
0.0498	1.85	1.81	1.64	1.31	0.75
0.0249	1.85	1.81	1.66	1.39	0.96
0.0124	1.85	1.82	1.68	1.40	1.01
0.0062	1.85	1.82	1.69	1.43	1.11

Table 3 Example 3, rotating hump: L^2-error of the solution of the **projection scheme** (41) with explicit Euler method for different discretization parameters timestep τ (rows) and mesh size h (columns).

$\tau\backslash h$	0.420	0.210	0.105	0.052	0.026
1.5707	1.85	1.87	1.94	1.88	2.33
0.7853	1.84	1.61	1.52	1.73	1.84
0.3926	1.83	1.71	1.01	0.56	0.51
0.1963	1.84	1.74	1.22	0.67	0.25
0.0997	1.84	1.78	1.50	0.86	0.34
0.0498	1.84	1.80	1.59	1.20	0.56
0.0249	1.85	1.81	1.62	1.28	0.81
0.0124	1.85	1.81	1.66	1.40	0.99
0.0062	1.85	1.82	1.67	1.43	1.10

Table 4 Example 3, rotating hump: L^2-error of the solution of the **projection scheme** (41) with explicit midpoint method for different discretization parameters timestep τ (rows) and mesh size h (columns).

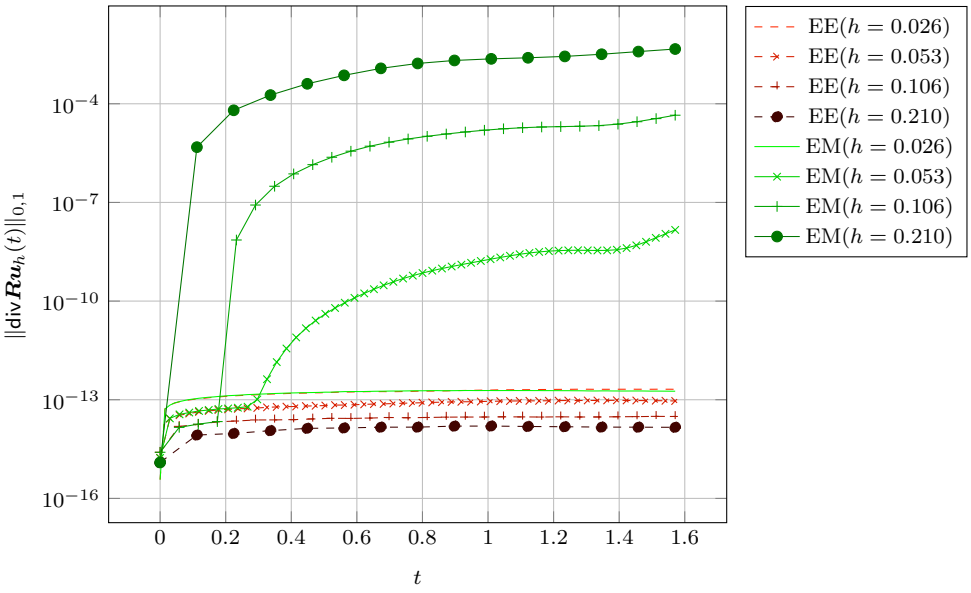

Fig. 7 Example 3: Behavior of $\|\mathsf{div}\boldsymbol{R}\boldsymbol{u}_h\|_{0,1}$ as a function of t, with $\boldsymbol{u}_h$ produced by the interpolation scheme with explicit midpoint rule (EM) and explicit Euler (EE) on meshes with different mesh sizes for the time intervall $[0, 0.5\pi]$.

the Euler method, because for the rotating flow the latter introduces a stronger drift towards the center, which completely offsets outward numerical diffusion.

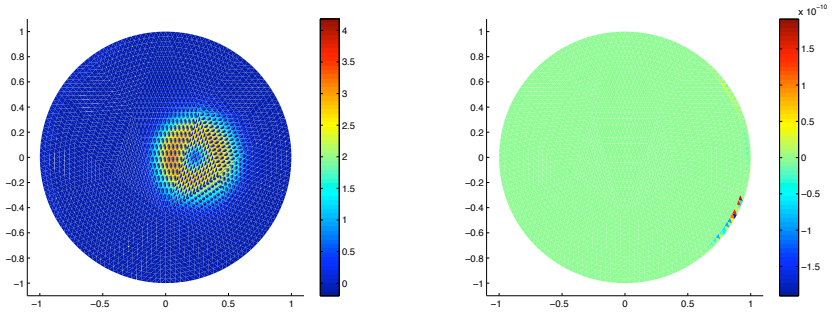

Fig. 8 Example 3: Plot of the modulus of $\boldsymbol{u}_h(0.5\pi)$ (left) and $\mathsf{div}\boldsymbol{R}\boldsymbol{u}_h(0.5\pi)$ (right), with $\boldsymbol{u}_h$ obtained by the interpolation scheme with explicit midpoint rule on a mesh with mesh size $h = 0.0521$ and $\kappa = 0.8$. Note the "div-pollution" emerging close to $\partial\Omega$.

References

1. D.A. Arnold, R.S. Falk, and R. Winther. Finite element exterior calculus: from Hodge theory to numerical stability. *Bull. Amer. Math. Soc.*, 47(2):281–354, 2010.
2. D.N. Arnold, R.S. Falk, and R. Winther. Finite element exterior calculus, homological techniques, and applications. *Acta Numerica*, 15:1–155, 2006.
3. David J. Benson. Computational methods in Lagrangian and Eulerian hydrocodes. *Comput. Methods Appl. Mech. Engrg.*, 99(2-3):235–394, 1992.
4. A. Bossavit. Discretization of electromagnetic problems: The "generalized finite differences". In W.H.A. Schilders and W.J.W. ter Maten, editors, *Numerical Methods in Electromagnetics*, volume XIII of *Handbook of numerical analysis*, pages 443–522. Elsevier, Amsterdam, 2005.
5. Alain Bossavit. Applied Differential Geometry. Lecture notes. Available online on http://butler.cc.tut.fi/ bossavit/BackupICM/Compendium.html, 2005.
6. Philippe G. Ciarlet. *The finite element method for elliptic problems*. North-Holland Publishing Co., Amsterdam, 1978. Studies in Mathematics and its Applications, Vol. 4.
7. John M. Dawson. Particle simulation of plasmas. *Rev. Mod. Phys.*, 55(2):403–447, 1983.
8. P. de Palma, G. Pascazio, G. Rosiello, and M. Napolitano. A second-order-accurate monotone implicit fluctuation splitting scheme for unsteady problems. *J. Comp. Phys.*, 208(1):1–33, 2005.
9. Jim Douglas, Jr. and Thomas F. Russell. Numerical methods for convection-dominated diffusion problems based on combining the method of characteristics with finite element or finite difference procedures. *SIAM J. Numer. Anal.*, 19(5):871–885, 1982.
10. Richard E. Ewing and Hong Wang. A summary of numerical methods for time-dependent advection-dominated partial differential equations. *J. Comput. Appl. Math.*, 128(1-2):423–445, 2001.
11. Theodore Frankel. *The geometry of physics : an introduction*. Cambridge: Cambridge University Press, 1998.
12. Morton E. Gurtin. *An introduction to continuum mechnaics*. Academic Press, 1981.
13. Philip Hartman. *Ordinary differential equations*. John Wiley & Sons Inc., New York, 1964.
14. H. Heumann, R. Hiptmair, and J. Xu. A semi-Lagrangian method for convection of differential forms. Report 2009-09, SAM, ETH Zürich, Zürich, Switzerland, 2009.

15. R. Hiptmair. Finite elements in computational electromagnetism. *Acta Numer.*, 11:237–339, 2002.
16. R. Hiptmair. Finite elements in computational electromagnetism. *Acta Numerica*, 11:237–339, 2002.
17. Paul Houston, Christoph Schwab, and Endre Süli. Discontinuous *hp*-finite element methods for advection-diffusion-reaction problems. *SIAM J. Numer. Anal.*, 39(6):2133–2163, 2002.
18. T. J. R. Hughes and A. Brooks. A multidimensional upwind scheme with no crosswind diffusion. In *Finite element methods for convection dominated flows*, volume 34 of *AMD*, pages 19–35. Amer. Soc. Mech. Engrs. (ASME), New York, 1979.
19. Serge Lang. *Differential and Riemannian manifolds*, volume 160 of *Graduate Texts in Mathematics*. Springer-Verlag, New York, third edition, 1995.
20. Serge Lang. *Fundamentals of Differential Geometry*. Springer, 1999.
21. P. Lasaint and P.-A. Raviart. On a finite element method for solving the neutron transport equation. In *Mathematical aspects of finite elements in partial differential equations*, pages 89–123. Math. Res. Center, Univ. of Wisconsin-Madison, Academic Press, New York, 1974.
22. K. W. Morton, A. Priestley, and E. Süli. Stability of the Lagrange-Galerkin method with nonexact integration. *RAIRO Modél. Math. Anal. Numér.*, 22(4):625–653, 1988.
23. K. W. Morton and E. Süli. Evolution-Galerkin methods and their supraconvergence. *Numer. Math.*, 71(3):331–355, 1995.
24. J.-C. Nédélec. Mixed finite elements in $\mathbf{R}^3$. *Numer. Math.*, 35(3):315–341, 1980.
25. J.-C. Nédélec. A new family of mixed finite elements in $\mathbf{R}^3$. *Numer. Math.*, 50(1):57–81, 1986.
26. O. Pironneau. On the transport-diffusion algorithm and its applications to the Navier-Stokes equations. *Numer. Math.*, 38(3):309–332, 1981/82.
27. A. Priestley. Exact projections and the Lagrange-Galerkin method: a realistic alternative to quadrature. *J. Comput. Phys.*, 112(2):316–333, 1994.
28. W.H. Reed and T.R. Hill. Triangular mesh methods for the neutron transport equation. Tech. Rep. LA-UR-73-479, Los Alamos National Laboratory, Los Alamos, NM, 1973.
29. R. N. Rieben, D. A. White, B. K. Wallin, and J. M. Solberg. An arbitrary Lagrangian-Eulerian discretization of MHD on 3D unstructured grids. *J. Comput. Phys.*, 226(1):534–570, 2007.
30. Günter Scheja and Uwe Storch. *Lehrbuch der Algebra. Teil 2*. Mathematische Leitfäden. B. G. Teubner, Stuttgart, 1988.
31. A. Staniforth and J. Côté. Semi-Lagrangian integration schemes for atmospheric models: A review. *Monthly Weather Review*, 119:2206–2223, 1991.
32. Endre Süli. Convergence and nonlinear stability of the Lagrange-Galerkin method for the Navier-Stokes equations. *Numerische Mathematik*, 53:459–483, 1988.

Research Reports

No.	Authors/Title
11-21	*H. Heumann, R. Hiptmair, K. Li and J. Xu* Semi-Lagrangian methods for advection of differential forms
11-20	*A. Moiola* Plane wave approximation in linear elasticity
11-19	*C.J. Gittelson* Uniformly convergent adaptive methods for parametric operator equations
11-18	*E. Kokiopoulou, D. Kressner, M. Zervos and N. Paragios* Optimal similarity registration of volumetric images
11-17	*D. Marazzina, O. Reichmann and Ch. Schwab* *hp*-DGFEM for Kolmogorov-Fokker-Planck equations of multivariate Lévy processes
11-16	*Ch. Schwab and A.M. Stuart* Sparse deterministic approximation of Bayesian inverse problems
11-15	*A. Barth and A. Lang* Almost sure convergence of a Galerkin–Milstein approximation for stochastic partial differential equations
11-14	*X. Claeys* A single trace integral formulation of the second kind for acoustic scattering
11-13	*W.-J. Beyn, C. Effenberger and D. Kressner* Continuation of eigenvalues and invariant pairs for parameterized nonlinear eigenvalue problems
11-12	*C.J. Gittelson* Adaptive stochastic Galerkin methods: beyond the elliptic case
11-11	*C.J. Gittelson* An adaptive stochastic Galerkin method
11-10	*C.J. Gittelson* Stochastic Galerkin approximation of operator equations with infinite dimensional noise
11-09	*R. Hiptmair, A. Moiola and I. Perugia* Error analysis of Trefftz-discontinuous Galerkin methods for the time-harmonic Maxwell equations